Electronic Supplementary Material (ESI) for Journal of Materials Chemistry A.

Supplementary Information

Enabling Efficient Visible Light Photocatalytic Water Splitting over $SrTaO_2N$ by incorporating Sr at B site

Xiaoqin Sun[a], Fangfang Wu[a], Gang Liu[b] and Xiaoxiang Xu[a,*]

[a]*Shanghai Key Lab of Chemical Assessment and Sustainability, School of Chemical Science and Engineering, Tongji University, 1239 Siping Road, Shanghai, 200092, China, *Email: xxxu@tongji.edu.cn, telephone: +86-21-65986919*

[b]*Shenyang National laboratory for Materials Science, Institute of Metal Research, Chinese Academy of Science, 72 Wenhua Road, Shenyang 110016, China*

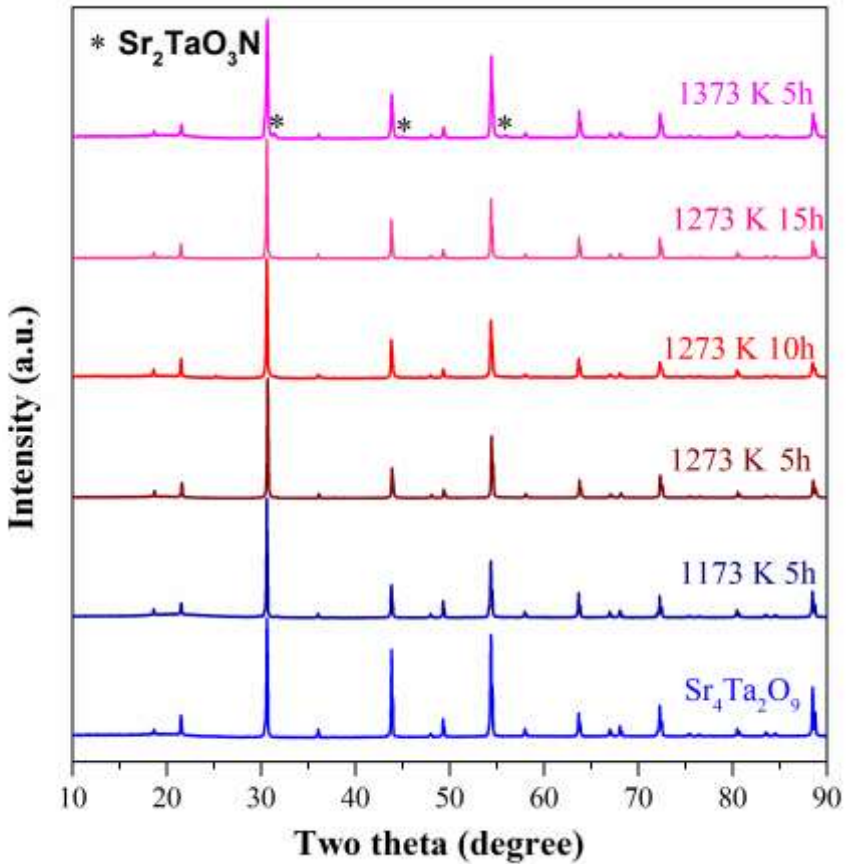

Figure S1. X-ray powder diffraction patterns of $Sr_4Ta_2O_9$ ammonolyzed at different temperatures and duration time, pristine $Sr_4Ta_2O_9$ is also included for comparisons. Impurity reflections are indicated by asterisk (*).

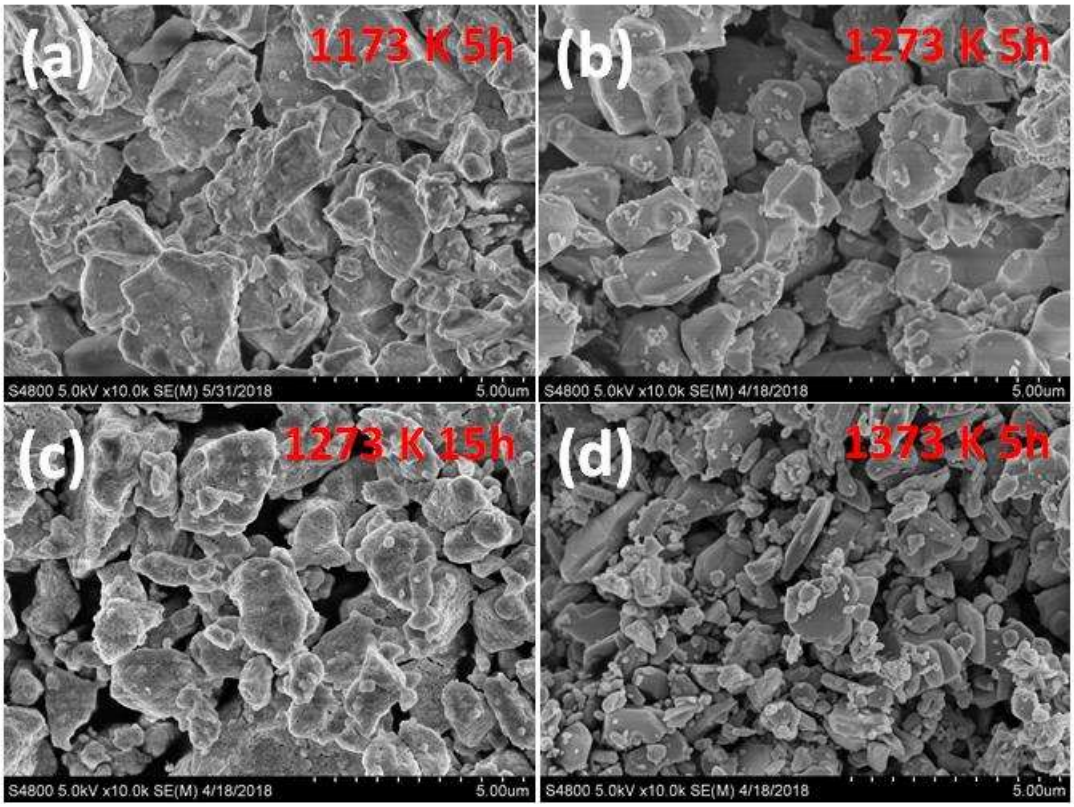

Figure S2. Field emission scanning electron microscopy images of $Sr_4Ta_2O_9$ ammonolyzed at different temperatures and duration time: (a) 1173 K 5h, (b) 1273 K 5 h, (c) 1273 K 15 h, and (d) 1373 K 5 h.

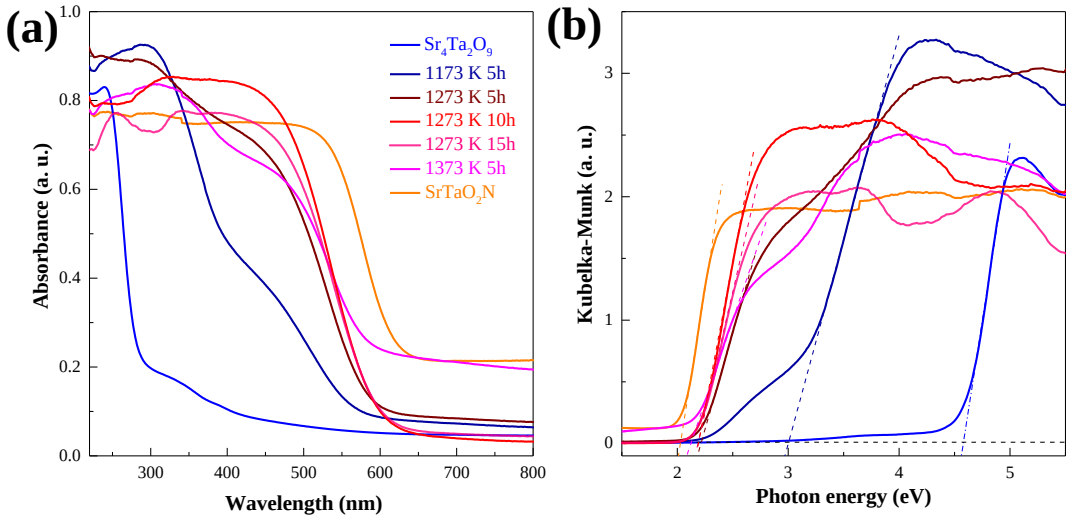

Figure S3. (a) UV–vis absorption spectra (converted from diffuse reflectance spectra) of $Sr_4Ta_2O_9$ ammonolyzed at different temperatures and duration time; (b) Kulbelka-Munk transformation of diffuse reflectance data, band gap values are determined by extrapolating the linear part of the curves down to energy axis.

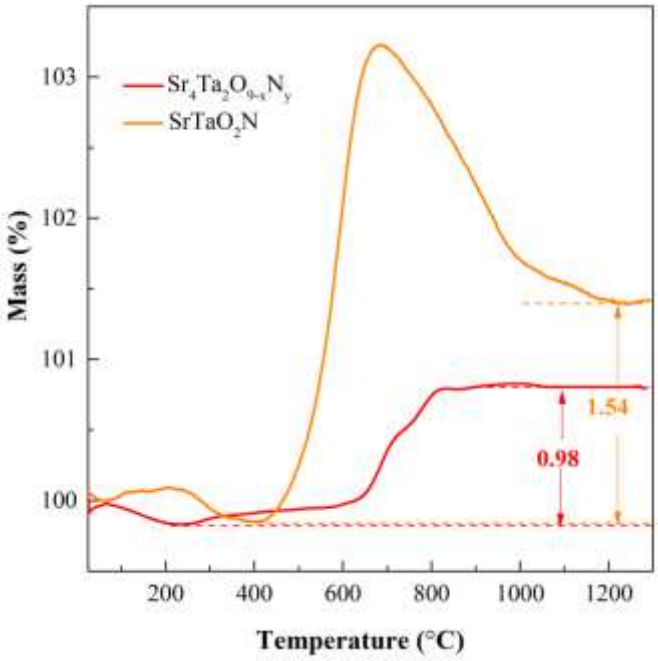

Figure S4. TGA curves of $Sr_4Ta_2O_{9-x}N_y$ and $SrTaO_2N$ in air with a heating rate of 10 K min^{-1}

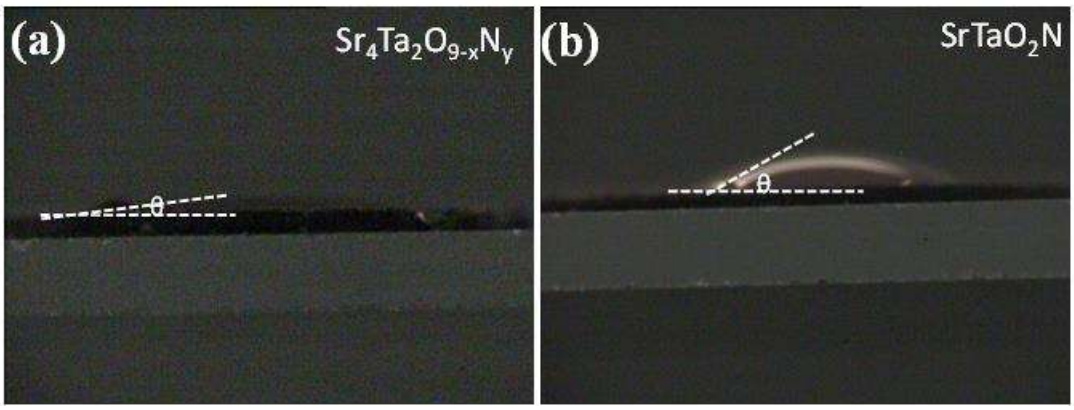

Figure S5. The dynamic contact angles of distilled water drop on pellets pressed by freshly prepared samples: (a) $Sr_4Ta_2O_{9-x}N_y$ and (b) $SrTaO_2N$.

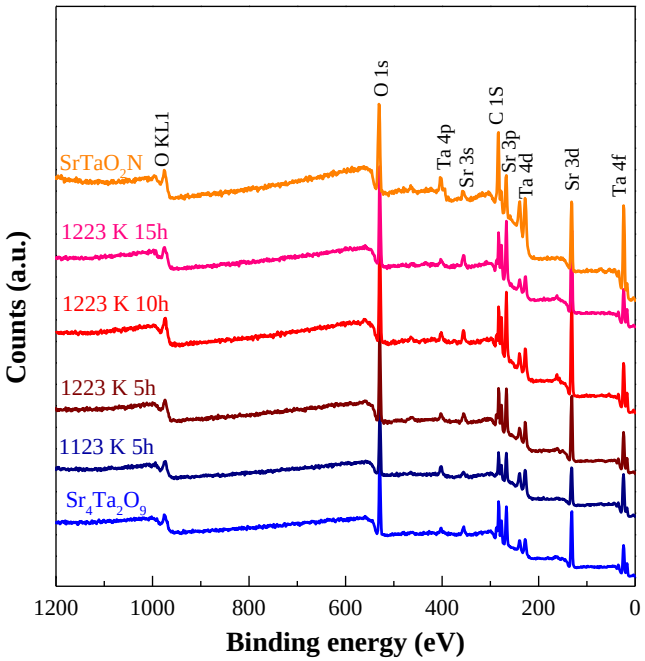

Figure S6. XPS survey spectra of all samples.

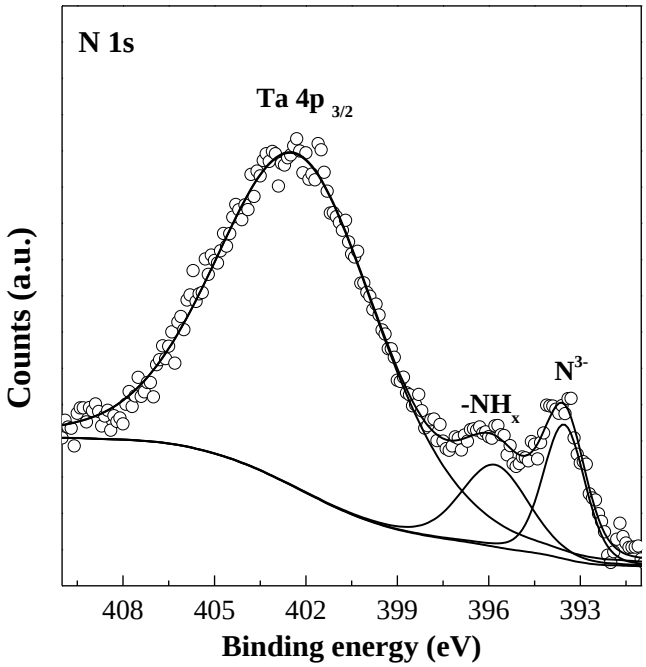

Figure S7. X-ray photoelectron spectra of N 1s state after *in situ* Ar ion sputtering $Sr_4Ta_2O_{9-x}N_y$ with beam energy of 4 keV for 150 s.

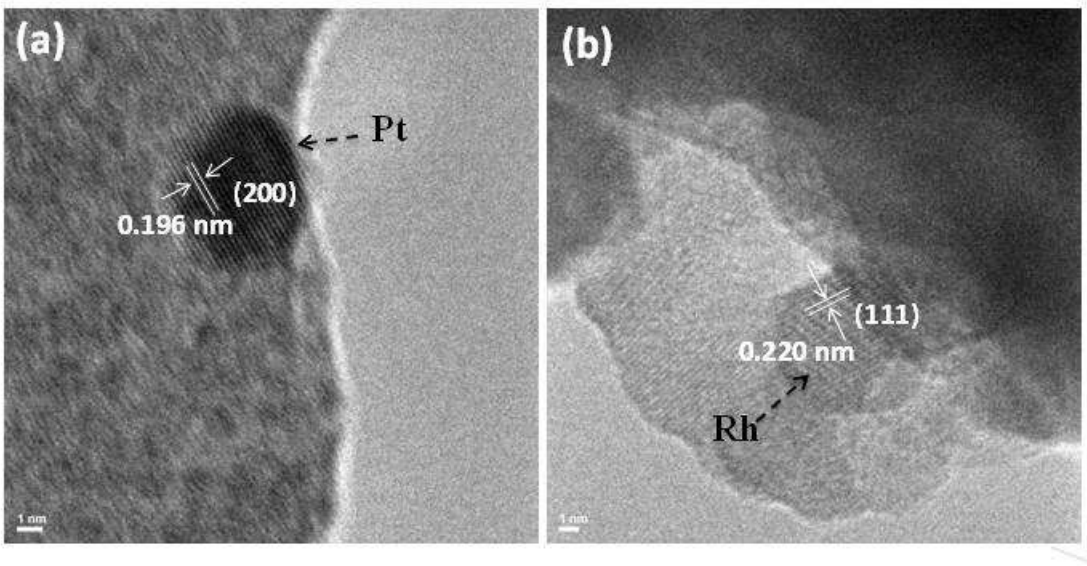

Figure S8. High resolution transmission electron microscopy (TEM) images of $Sr_4Ta_2O_{9-x}N_y$ loaded with Pt (a) and $Rh@Rh_2O_3$ (b).

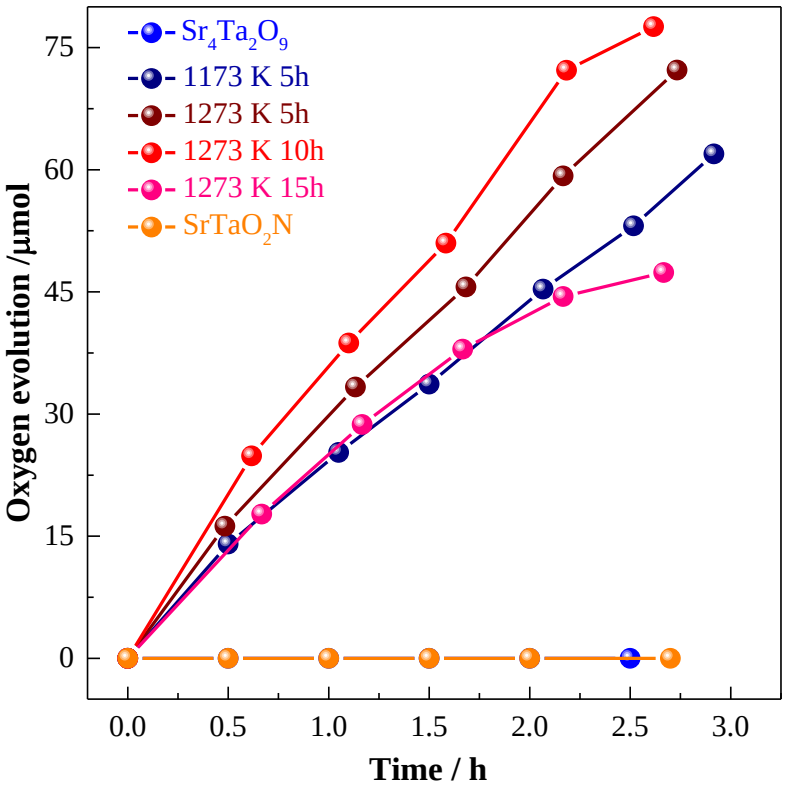

Figure S9. Photocatalytic oxygen production of $Sr_4Ta_2O_9$ ammonolyzed at different temperatures and duration time in the presence of silver nitrate aqueous solution (0.05 M), 1 wt% $Rh@Rh_2O_3$ was loaded as the cocatalyst

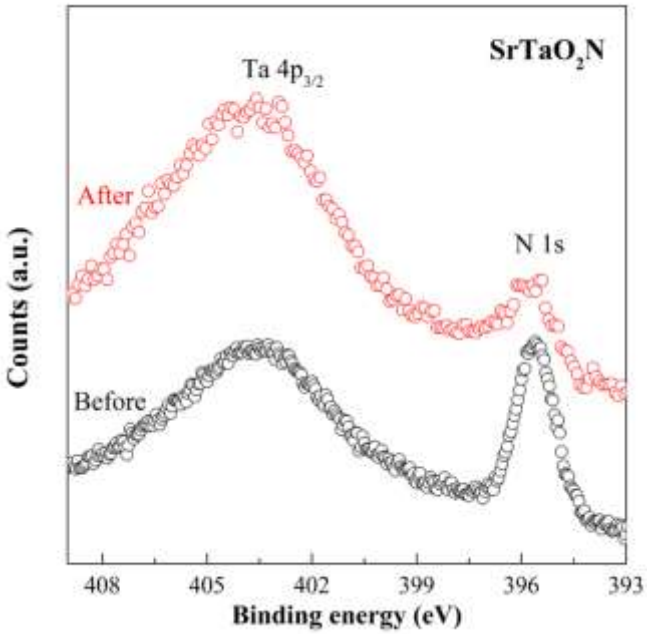

Figure S10. X-ray photoelectron spectroscopy (XPS) of N 1s state for $SrTaO_2N$ before and after photocatalytic reaction.

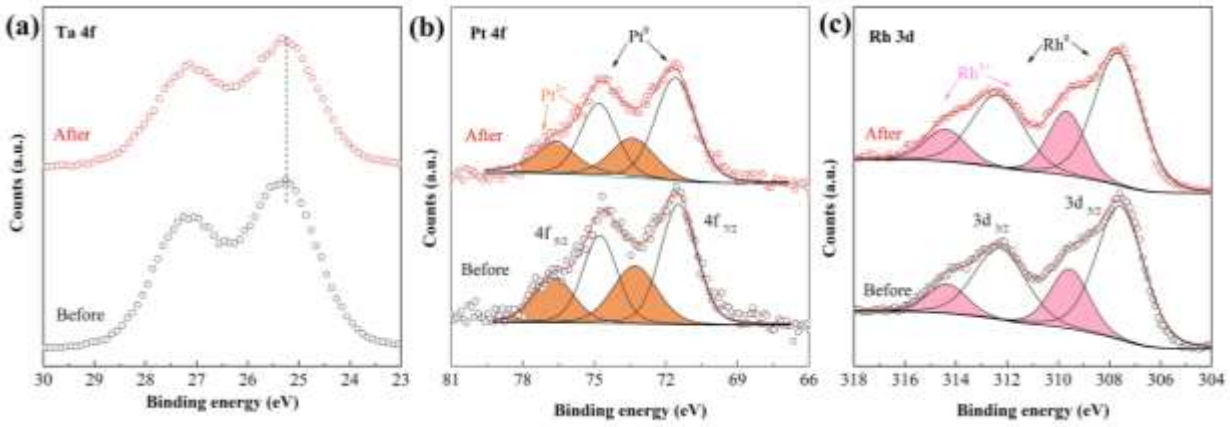

Figure S11. X-ray photoelectron spectroscopy (XPS) of $Sr_4Ta_2O_{9-x}N_y$ before and after photocatalytic reaction: (a) Ta 4f state, (b) Pt 4f state, and (c) Rh 3d state, respectively.

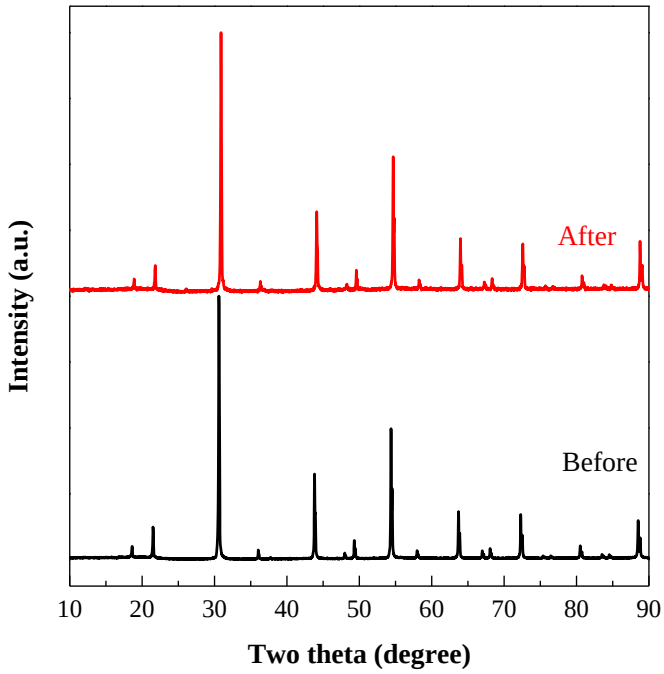

Figure S12. X-ray powder diffraction patterns of $Sr_4Ta_2O_{9-x}N_y$ before and after photocatalytic reactions.

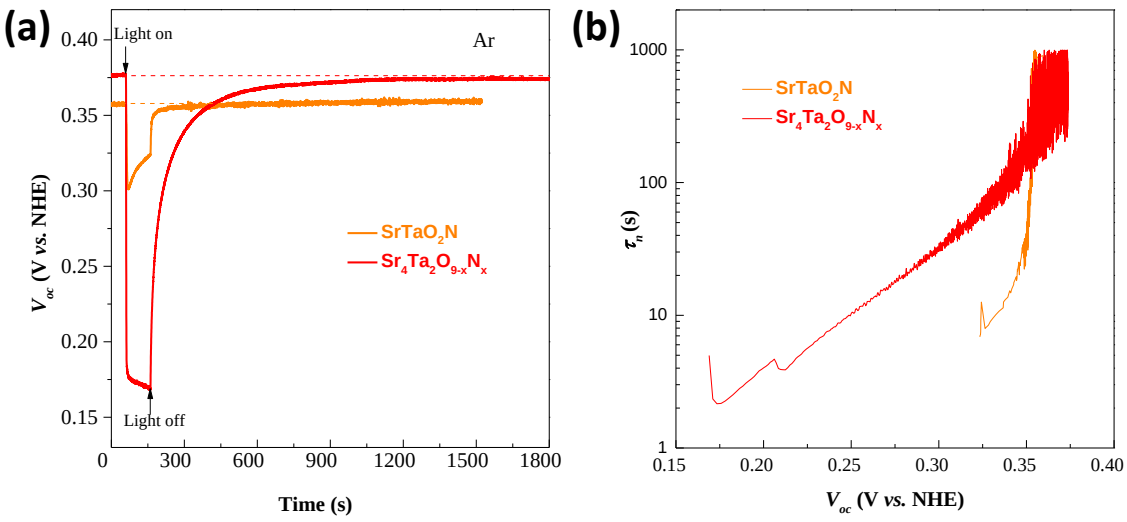

Figure S13. (a) V_{oc} time profile of $SrTaO_2N$ and $Sr_4Ta_2O_{9-x}N_y$ in Ar atmosphere, illumination ($\lambda \geq 400$ nm) started after a steady V_{oc} was achieved in the dark and was terminated after 100 s, (b) electron lifetime derived from Equation S1 (see information below).

Open-circuit voltage decay (OCVD) experiments can be used to evaluate the charge separation conditions inside a semiconductor and electron lifetime. The steady state V_{oc} in the dark is immediately dropped down upon light illumination due to consumption of photo-generated holes at the semiconductor surface and simultaneous accumulation of photo-generated electrons[1]. This negatively shifts Fermi level of semiconductors as well as V_{oc}. Instantaneously removing illumination of photo-electrodes results in decay of V_{oc} which is governed by various electron dissipation pathways (e.g. recombined with trapped holes, etc.). This provides a direct evaluation of charge separation situations inside semiconductors. The lifetime of these accumulated electrons can be quantitatively approximated using the following

equation[2]:

$$\tau_n = \frac{k_B T}{e}\left(\frac{dV_{oc}}{dt}\right)^{-1} \quad \text{(S1)}$$

where τ_n is potential dependent lifetime, k_B is Bolzmann's constant, T is the temperature in K and e is the elementary charge. $Sr_4Ta_2O_{9-x}N_y$ shows a much slower V_{oc} decay profile and a much longer electron lifetime compared to $SrTaO_2N$, which explains its superior photocatalytic activity compared with pristine $SrTaO_2N$.

Table S1. The moles of photon flux per hour gauged by a quantum meter (Apogee MP-300) and photocatalytic oxygen production rate of $Sr_4Ta_2O_{9-x}N_y$ under monochromic light illumination.

λ /nm	Flux / μmol·h^{-1}	O_2 evolution / μmol·h^{-1}
600 ± 40	2895	1.41
550 ± 35	2447	3.06
500 ± 35	1925	5.21
450 ± 35	1255	8.05
420 ± 20	1147	9.82

Table S2. Contact angle, Zeta-potential, and the refined cationic composition

Samples	Contact angle (degree)	Zeta-potential (mV)	the refined ratio Sr/Ta
$Sr_4Ta_2O_{9-x}N_y$	7	-14.9	1.97
$SrTaO_2N$	25	-10.0	1.01

Table S3. The binding energy (BE) and full width at half maximum (FWHM) of Ta $4f_{7/2}$ and $4f_{5/2}$ by peak-fitting XPS spectra

Samples	Ta $4f_{5/2}$		Ta $4f_{7/2}$	
	BE (eV)	FWHM (eV)	BE (eV)	FWHM (eV)
$Sr_4Ta_2O_9$	25.28	1.54	27.15	1.49
1173 K 5h	25.2	1.67	27.12	1.62
1273 K 5h	25.34	1.53	27.24	1.49
1273 K 10h	25.28	1.50	27.15	1.48
1273 K 15h	25.23	1.52	27.22	1.47
1373 K 5h	24.29 / 25.32	1.30 / 1.39	26.21 / 27.16	1.11 / 1.35
$SrTaO_2N$	24.53 / 25.53	1.48 / 1.28	26.48 / 27.37	1.20 / 1.23

References

1. B. H. Meekins and P. V. Kamat, *ACS Nano*, 2009, **3**, 3437-3446.
2. A. Zaban, M. Greenshtein and J. Bisquert, *ChemPhysChem*, 2003, **4**, 859-864.